4ICEGE Thessaloniki-GREECE 2007

4th International Conference on
Earthquake Geotechnical Engineering
June 25-28, 2007
Paper No. 1393

EFFECT OF A LIQUEFIABLE SOIL LAYER ON SOIL-STRUCTURE INTERACTION AND BUILDING DAMAGE

Panos DAKOULAS [1], George KALYVAS[2], Polynikis VAZOURAS[2]

ABSTRACT

The seismic behaviour of a typical actual 7-storey reinforced-concrete building is investigated to assess the effect of the presence of a liquefiable soil layer. The building has been designed on the basis of the low ductility requirements of earlier seismic codes and assumed to be founded at four actual sites. The first site is the typical soil profile, which represents average values of soil properties of the seismic zone. The other three sites are also located within the same zone and each contains a liquefiable soil layer, with relative density 60%, 50% and 40%, respectively. The results show that the presence of a liquefiable layer may significantly affect the seismic damage of the structure. The building investigated experienced tolerable deformations at the typical soil profile. However, at the sites containing the liquefiable layer, the same building developed significant seismic damage in terms of interstorey drift. In addition, substantial plastic deformation and bending developed in many beams of the building, especially between the ground floor and the third floor.

Keywords: Liquefaction, Soil–Structure Interaction, Seismic Response, Building Damage.

INTRODUCTION

The seismic behavior of older multi-story reinforced-concrete buildings, designed on the basis of the low ductility requirements of earlier seismic codes, is of significant interest as it affects the safety of a large proportion of buildings worldwide. In Greece, buildings designed using the seismic code of 1985 (or earlier) may have a natural ductility $\mu_{\Delta} \approx 2.5$ and, therefore, posses a limited capacity to sustain large deformations. If founded on soils that may contain a liquefiable layer, such structures may experience significant seismic damage. The objective of this study is to examine the effects of the presence of a liquefiable foundation soil layer on the seismic damage of such buildings.

To this end, the study examines the seismic behavior of a rather typical 7-story building that has been designed according to the outdated Greek Seismic Code of 1985. The same building is assumed to be founded on four different soil profiles located at the center of the city of Larissa, Greece. The first building is founded on a typical soil profile, i.e. having average shear wave velocities, of a certain seismic zone at the city center. The other three buildings are assumed to be founded on soil profiles at specific sites in the same seismic zone, each containing a liquefiable layer of different relative density. These four soil-structure systems are subjected to a series of seismic excitations that have the characteristics of the design earthquake for that region. The response and the seismic damage of the four systems are examined in order to assess the effect of the presence of the seismic layer.

Before proceeding with the analysis of the soil – structure system, it is of interest to examine first the site seismic response assuming free field conditions.

[1] Associate Professor, Department of Civil Engineering, University of Thessaly, Volos, Greece, Email: dakoulas@uth.gr
[2] Graduate Student, Department of Civil Engineering, University of Thessaly, Volos, Greece.

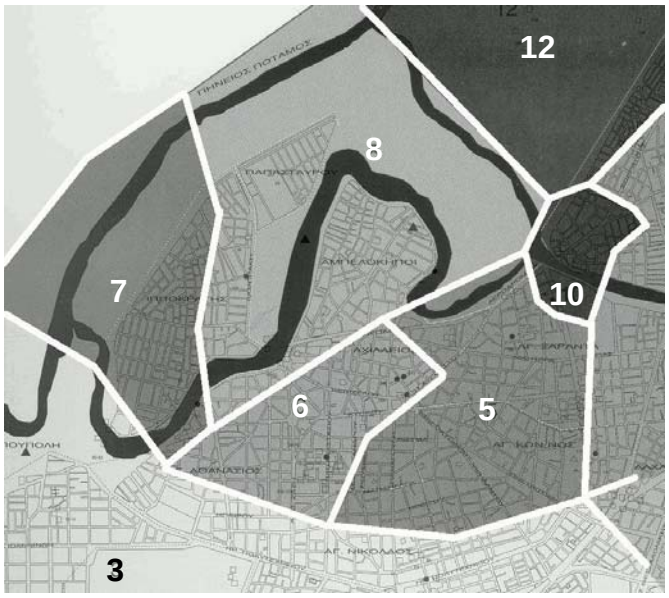

Figure 1. Seismic zones at the centre of the City of Larissa

SITE SEISMIC RESPONSE

Seismological data

According to the current Greek Seismic Code, the effective peak ground acceleration (PGA) for the City of Larissa is 0.24 g with a 10% probability of exceedance in 50 years. A seismic hazard analysis study for the city (Pitilakis and Tsotsos 1995) has proposed two scenarios, one for a near field source and one for a far field source. The characteristics of the two seismic scenarios are given in Table 1. The aforementioned study divides the city in a total of 18 geo-seismic zones. The present study focuses on Zone 6, located at the city center shown in Fig. 1. The typical soil profile of this zone is subjected to ten seismic excitations, utilizing the historic records given in Table 2, properly scaled to the expected peak ground acceleration.

Table 1. Seismic Scenarios

Seismic Scenario	A	B
Earthquake Magnitude, Ms	7	6.3
Epicentral Distance, R	80 km	6 – 10 km
Peak Ground Acceleration	0.20 g	0.335 g

Table 2. Earthquake Excitations

Number	Earthquake	Year	Scenario
1	Almyros	1987	A
2	Edessa No. 1	1990	A
3	Edessa No. 2	1990	A
4	Kilkis	1990	A
5	Kobe	1995	A
6	Aigio	1995	B
7	El Centro	1940	B
8	Ierissos	1983	B
9	Kalamata	1986	B
10	Ouranoupolis	1983	B

Soil profile and site response at Zone 6

Fig. 2(a) shows the typical soil profile at Zone 6. The soil profile consists of a 10 m thick layer of fill, a 3 m thick layer of clay, a 4 m thick layer of silty sand and silt, a 10 m thick layer of clay, a 10 m thick layer of silty sand and silt, and a very deep layer of clay. Fig. 2(b) plots the distribution of the shear wave velocity versus depth at Zone 6. At depths greater than -100 m, the material is assumed to be equivalent to bedrock having a shear wave velocity V_S = 800 m/s. The initial fundamental period of the site is T_1 = 0.88 seconds.

The site response is evaluated using 1-D equivalent linear analysis. The variation of the shear modulus ratio and the critical damping ratio with the amplitude of cyclic shear strain is based on laboratory data by Pitilakis and Tsotsos (1995). Figs. 3(a) and (b) plot the distribution with depth of peak accelerations and peak shear strains, respectively, experienced during shaking by the ten excitations listed in Table 2. The peak accelerations at the ground surface range from 0.30 g to 0.44 g.

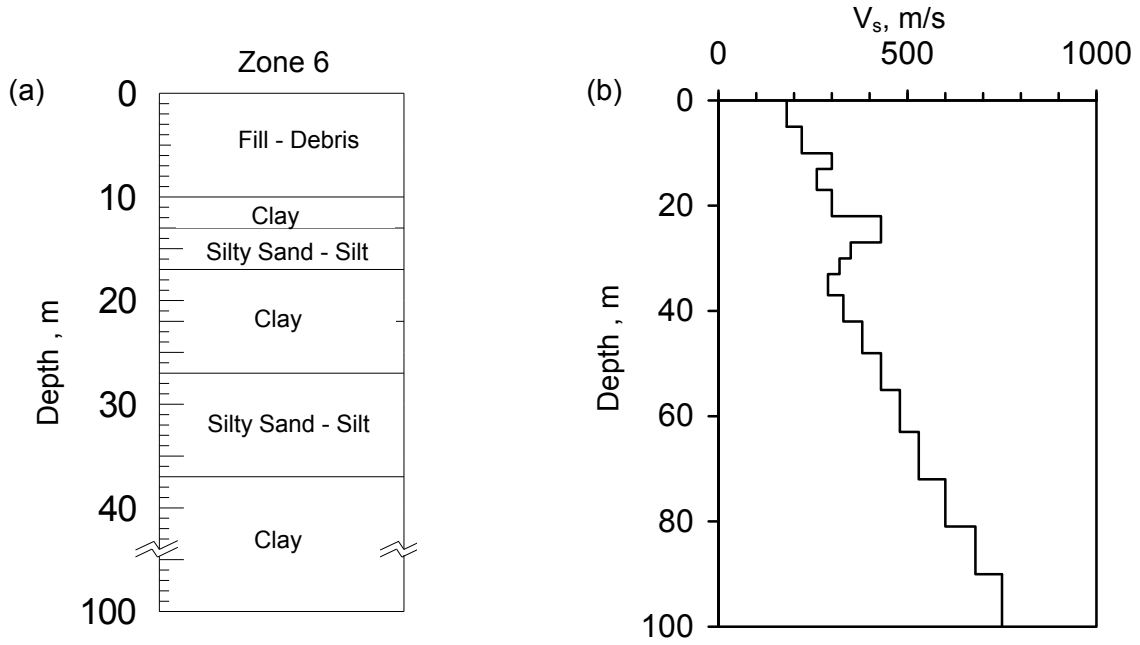

Figure 2. (a) Soil profile and (b) S-wave velocity vs depth at Zone 6 (Pitilakis & Tsotsos 1995)

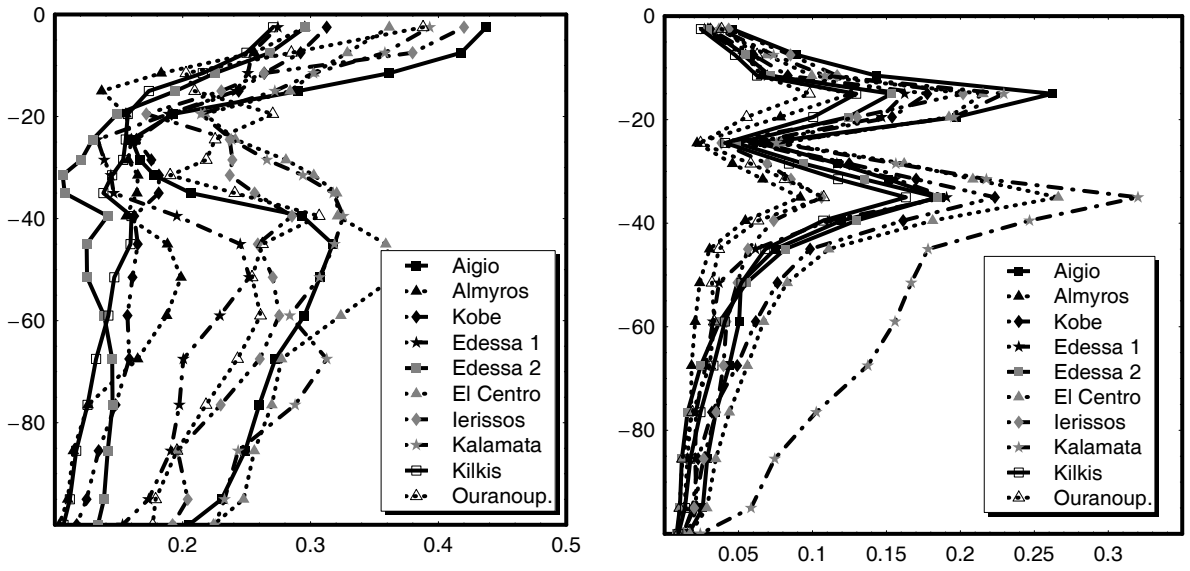

Figure 3. (a) Acceleration and (b) shear strain versus depth for ten excitations at Zone 6

Soil and structure discretization

The seismic analysis is performed using the program FLAC (Itasca 2000) and an appropriate elasto-plastic model for the cyclic behaviour of cohesionless soils. A typical discretization of the soil profile – structure system is portrayed in Fig. 4(a), in which the thickness of the individual soil layers may vary to represent the soil profile at a given site and is taken less than $\lambda_{min}/8$, where λ_{min} is the minimum wave length of the excitation. The building consists of a basement of 4 m depth, a ground floor of 6 m height, and six additional floors of 3 m height each. The foundation consists of a mat with connecting beams. The building is discretized as a 2-D structure by considering an equivalent frame section along its shorter side. The frame consists of 5 columns, as shown in Fig. 4(b). The beams and columns of the building are modelled as elastic-plastic members. Fig. 4(c) plots representative relationships between the ultimate moment and the axial force at various floor levels for columns K2 and K4. It is noted that the concrete strength reduction due to cracking and the shear failure are ignored.

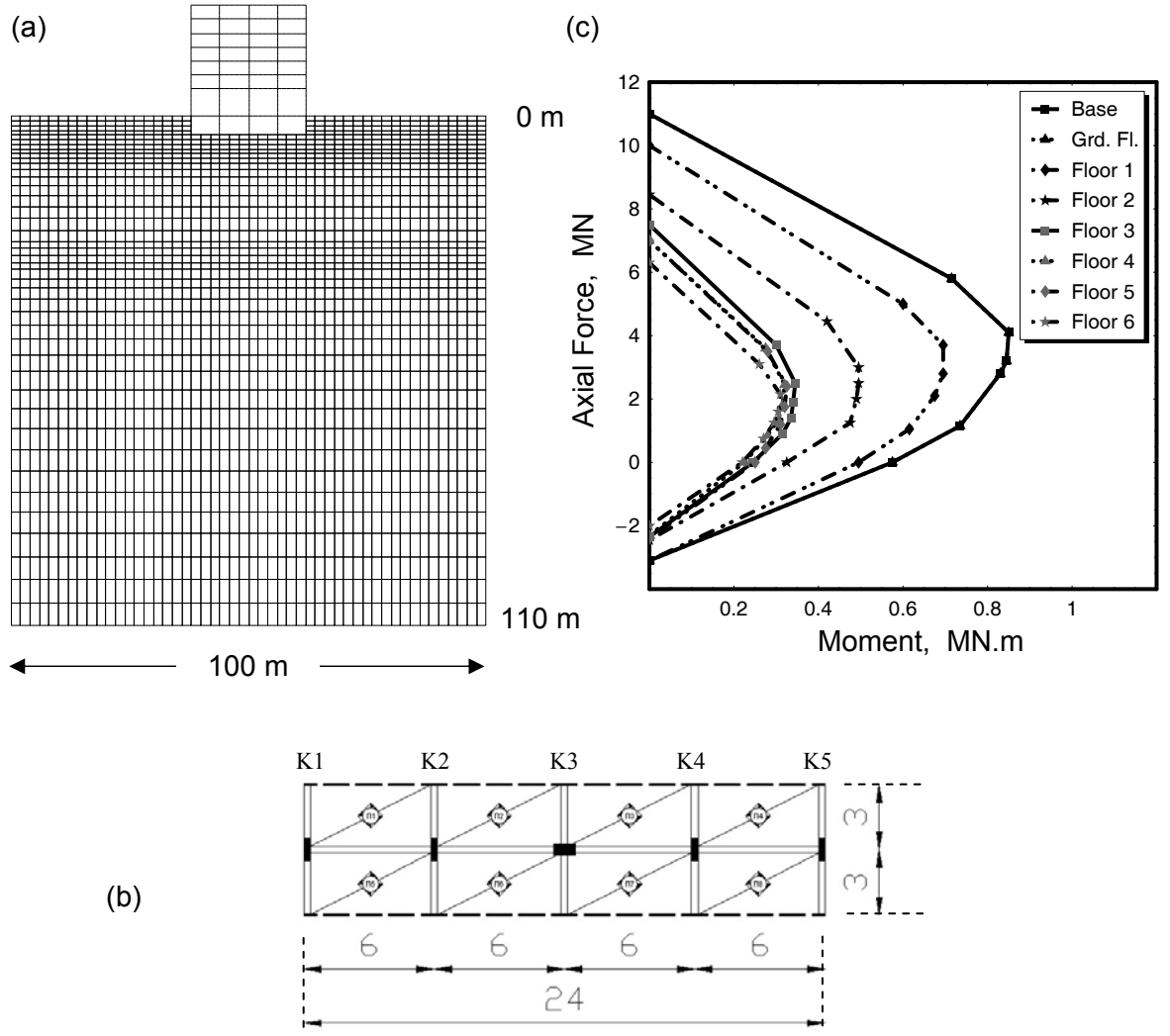

Figure 4. (a) Soil and structure discretization (b) equivalent frame section for 2-D analysis and (c) relation of ultimate moment and axial force at various floor levels for columns K2 and K4.

Soil Constitutive Model for cohesionless soil

The effective stress analysis is utilized for the simulation of the development of excess pore water pressures and liquefaction, based on full coupling of the volumetric changes of the soil skeleton and the pore water. The constitutive model for cohesionless soil used in the present study is the model developed by Pastor *et al*. (1990), subject to minor modifications. The model is based on the generalized plasticity theory and can be used for the monotonic and cyclic behavior of cohesionless soil. In agreement with experimental evidence for such soils, it utilizes a non-associated flow rule. By contrast to classical plasticity, the model does not require the application of the consistency condition to define the hardening modulus. This simplifies considerably the computational aspects and improves the computational efficiency. Detailed descriptions of the basic model are given by Pastor *et al.* (1990) and Zienkiewicz *et al.* (1999). The stress strain relationship is given by:

$$d\sigma' = D^{ep}_{L/U} d\varepsilon = (D^e - \frac{D^e n_{gL/U}\, nD^e}{H_{L/U} + n^T D^e n_{gL/U}}) d\varepsilon \qquad (1)$$

where $d\sigma'$ = effective stress change, $d\varepsilon$ = strain increment, D^e = elastic stiffness matrix, $D^{ep}_{L/U}$ = elasto-plastic stiffness matrix, $H_{L/U}$ = plastic modulus for loading and unloading , n = unit vector normal to the loading surface, $n_{gL/U}$ = unit vector normal to the loading surface.

For loose *contractive* sand the model predicts the densification and strain hardening under drained shearing, and the development of excess pore pressure and liquefaction under undrained shearing. For very dense *dilative* sands in drained shear, the model accounts for strain softening and residual conditions at the critical state. Comparisons between predictions of the original model and experimental data on undrained monotonic loading of contractive and dilative sands, on cyclic loading leading to liquefaction of very loose sands, and on cyclic mobility of dense sands, showed very good agreement (Pastor *et al*. 1990).

The modified version utilized in the present study differs mainly in that it has pressure-dependent plastic moduli for both loading and unloading and that the plastic loading modulus depends on the Lode angle, taking into account the different soil response in compression and extension. Fig. 5(a) shows a comparison of the effective stress paths during triaxial undrained compression of Banding sand (Castro 1969) with relative density D_r = 29%, 44 %, 47 % and 64 % using the modified version, whereas Fig. 5(b) compares the corresponding excess pore water pressure versus shear strain. Fig. 6 compares of stress paths during undrained cyclic triaxial testing of a sample with relative density D_r =30 %. Finally, Fig. 7 compares the Cyclic Stress Ratio (CSR) for initiation of liquefaction in simple shear tests from model predictions and experimental data of Nevada Sand (Arulmoli *et al*. 1992) and Monterey Sand (DeAlba *et al*. 1976, as modified by Seed and Harder 1990) for relative densities of 40 % and 60 %. Moreover, a systematic series of comparisons between predictions of the modified model and experimental data of different sands from both monotonic and cyclic tests in compression-extension and simple shear showed very good agreement (Dakoulas 2003). The model seems capable of describing realistically soil behavior under monotonic and cyclic loading for a wide range of relative densities. It is being used here to simulate approximately the soil response under seismic conditions.

Building response at non-liquefiable profile of Zone 6

In this case the building is assumed to be founded on the typical soil profile of Zone 6 (see Fig. 2), in which no liquefaction is expected. Initially a static analysis is performed for the evaluation of the initial stresses. For the dynamic analysis of the soil – structure system, the elastic moduli and the critical damping ratios of the *non-liquefiable* soil layers are obtained from equivalent linear analysis, so that they are compatible with the amplitude of the seismic shear strains developing in each material element.

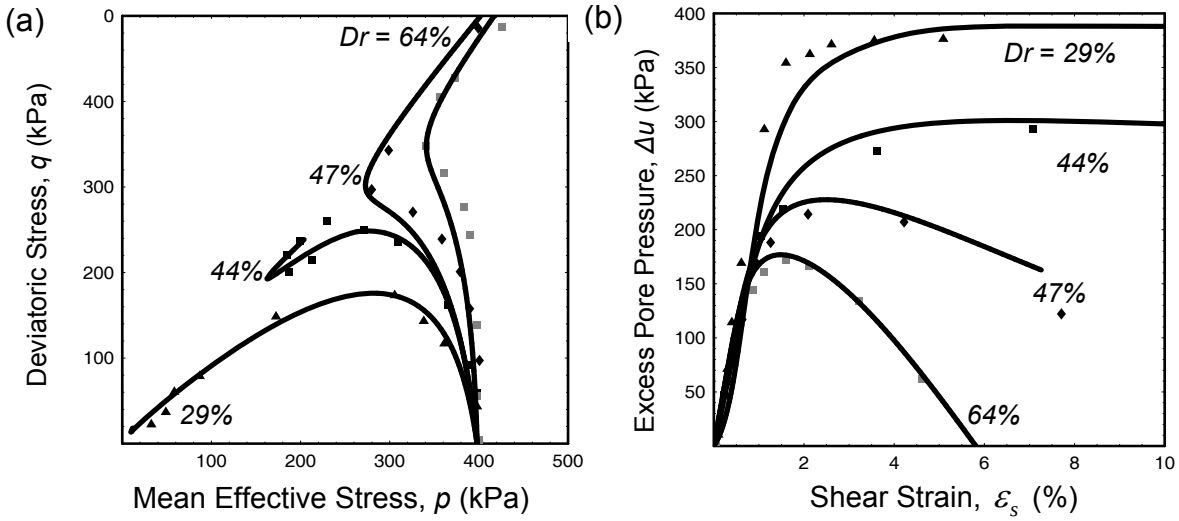

Figure 5. Comparison of experimental data from Castro (1969) with numerical simulations by the modified Pastor et al. (1990) model: (a) effective stress paths (b) excess pore pressures.

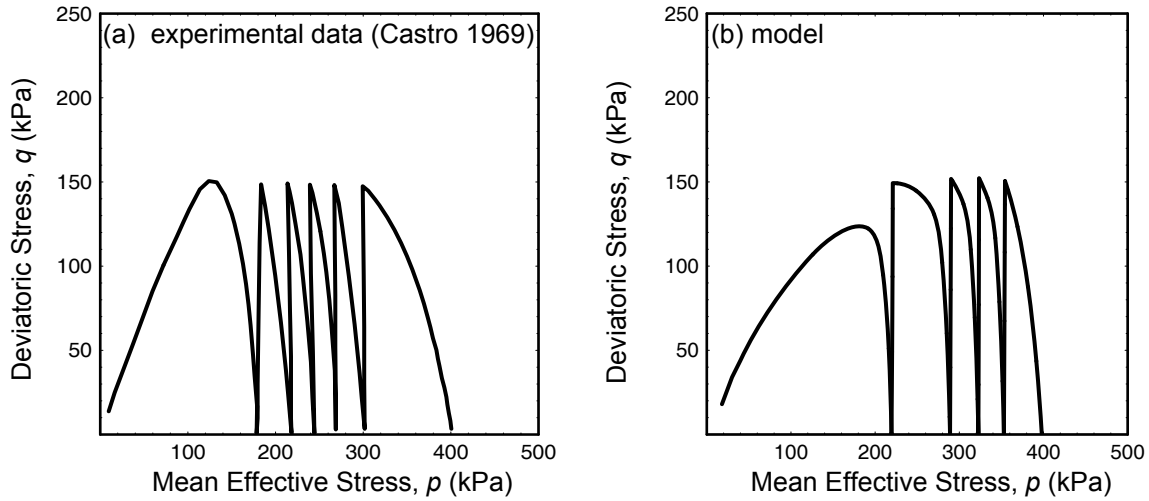

Figure 6. Effective stress paths in cyclic triaxial testing for a sand with D_r = 30%: (a) experimental data (Castro 1969) and (b) numerical prediction.

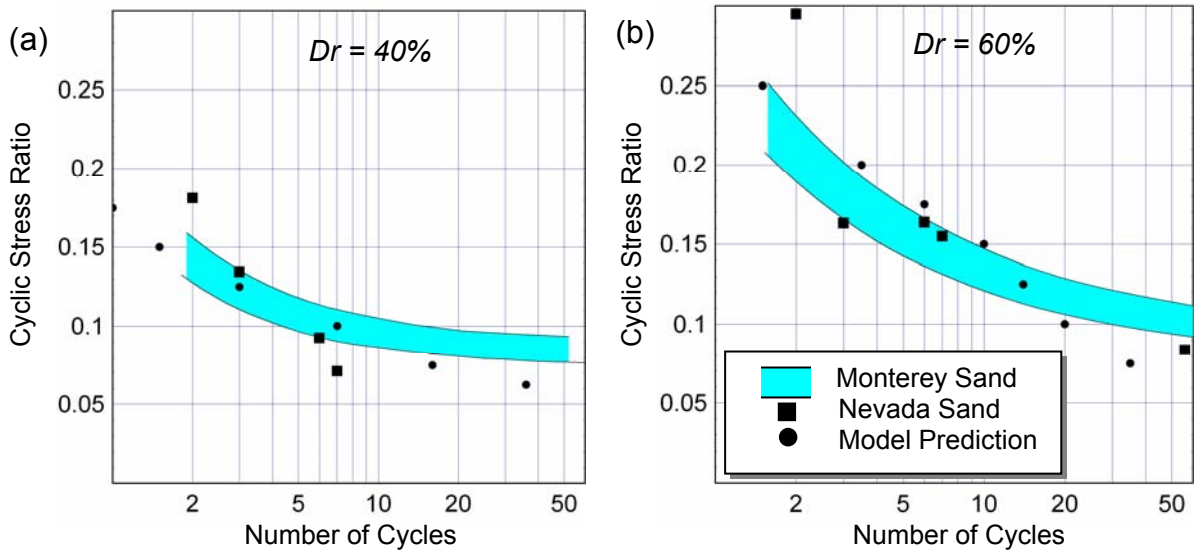

Figure 7: Cyclic Stress Ratio for initial liquefaction in simple shear tests from model predictions and experimental data for Nevada Sand (Arulmoli *et al.* 1992) and Monterey Sand (DeAlba *et al.* 1976, as modified by Seed and Harder 1990): (a) Dr = 40% and (b) Dr = 60%.

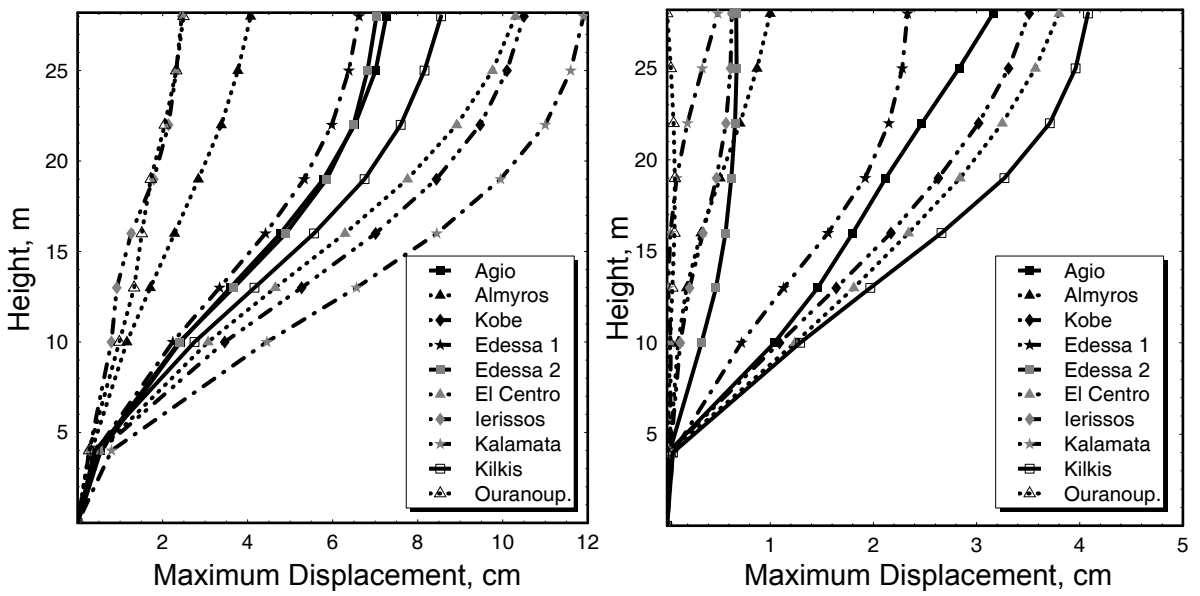

Figure 8: (a) Maximum relative displacements and (b) residual relative displacements along the height of the building at a site with typical properties of Zone 6 for 10 earthquake excitations.

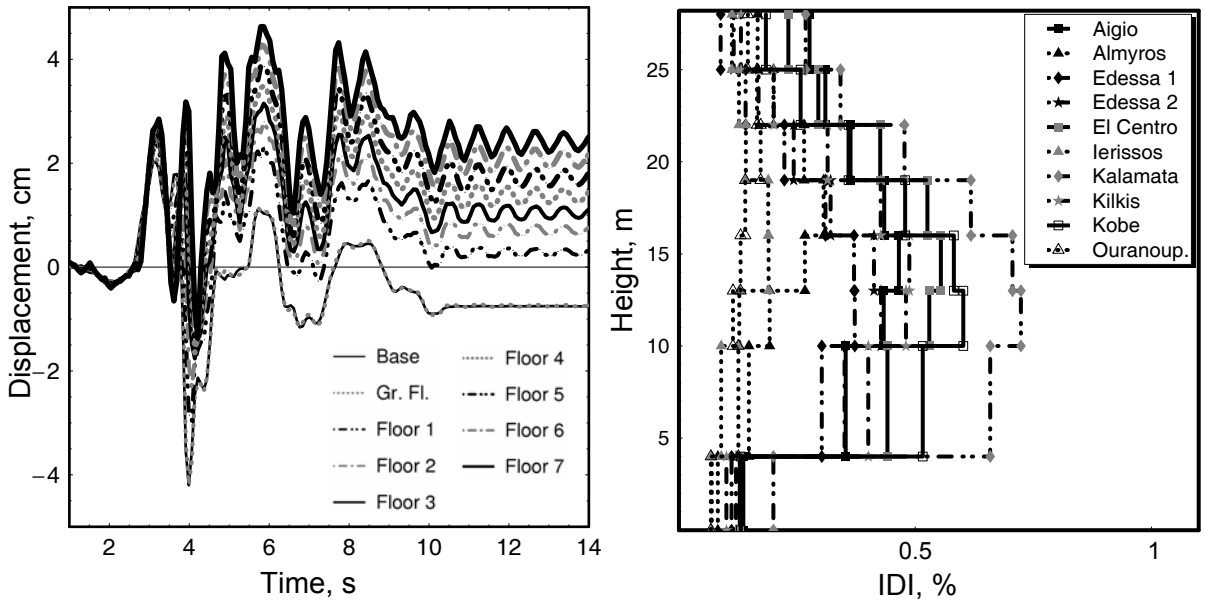

Figure 9: (a) Displacement time histories at various floor levels for the Aigio earthquake excitation and (b) Interstory Drift Index along the height of the building at a site with typical properties of Zone 6 for 10 earthquake excitations.

To account for the radiation of wave energy back into the bedrock material, the excitation is applied in terms of seismic shear stresses at the base of the soil-structure system. The free field response at the left and right side of the soil-structure mesh are simulated using two soil columns that are connected to the mesh with dashpots.

Figures 8(a) and 8(b) plot the maximum and residual horizontal relative displacements along the height of the building for the ten earthquake excitations. It is noted that the maximum value of the horizontal relative displacement is 12 cm, whereas the maximum value of the horizontal residual displacement is about 4 cm. Fig. 9(a) plots the displacement time history at various floor levels of the

building subjected to the Aigio seismic record. The corresponding accelerations (not shown here) at the top of the building vary from 0.5g to 0.8g, whereas at the base vary from 0.2g to 0.5g.

Figure 9(b) plots the distribution of the Interstory Drift Index (IDI), which is defined as the ratio of the maximum relative displacement between the ceiling and the base of a given floor over the height of that floor. Considering that the building has been designed with the natural ductility ($\mu_\Delta \approx 2.5$), the value of IDI should not exceed the value of 1% (Bachmann 1998). Note that the values of IDI in Fig. 9 remained significantly less that 1% and, therefore, the associated deformations are tolerable. Also, note that the maximum values of IDI developed between the ground floor and the third floor. A detailed examination of the behavior of the column and element connections has shown that plastic deformations developed in most of the connections of the superstructure. In this way, the dissipated seismic energy was distributed in a large portion of the building.

A limitation of the analysis is that it ignores the stiffness of the non-bearing walls. Such walls do not exist along the perimeter of ground floor. Instead, huge glass windows are placed, as they are preferred by the shop owners who use them. Hence, the building is simulated as almost fixed at the basement, and relatively more flexible than it is in reality from the first floor to the top. As a result it is expected that, being more flexible, the ground floor may experience a little higher deformation than the computed in this analysis.

Table 3. Characteristics and factors of safety for the three liquefiable layers

Site	A	B	C
Depth of layer, m	4.6 – 6 m	4 – 6.2 m	5 – 9 m
Soil type	SP - SW	SP - SW	SM - ML
N - SPT	12	8	3
Relative Density, Dr	≈ 60 %	≈ 50 %	≈ 40 %
Factor of Safety (NCEER)	0.83	0.62	0.71
Factor of Safety (JRA)	0.81	0.57	0.63

Building response at sites A, B and C of Zone 6

Fig. 10 portrays the soil profiles at sites A, B and C, which are located within Zone 6 and each contains a liquefiable layer. Table 3 gives the depth of the liquefiable layer, the soil type, the field N-SPT blow counts, and the estimated relative density for each of the three layers. Simplified analysis of the liquefaction potential using the NCEER Workshop method and the Japan Road Association method, which account for the influence of fines content and plasticity index, has shown that the factor of safety (FS) against liquefaction for the design earthquake is less than one. These values of FS are given also in Table 3 for the three sites.

Initially, the free field response at each site is computed, followed by the analysis of the soil – structure system. The soil – structure system mesh that is used for the analysis is similar to that in Fig. 4(a), with minor modifications in the thickness of specific soil layers. The *liquefiable* soil layers are modelled using the elasto-plastic constitutive model. The model parameters are computed based on the relative density of the soil, estimated by using the corrected N-SPT values and the grain size distribution characteristics. For computational efficiency, the *non-liquefiable* soil layers are modelled as linear elastic materials having strain-compatible dynamic properties derived from previous equivalent linear analysis. For the soil-structure system at site A, subjected to the Aigio acceleration record scaled at 0.33g, Fig. 11(a) plots the evolution of the excess pore water pressure ratio $\Delta u / \sigma'_{m0}$, where Δu = the excess pore pressure and σ'_{m0} = the mean effective stress. The ratio is evaluated at the middle of the soil layer, beneath the middle column of the building. Fig. 11(b) plots the distribution of the ratio within the soil layer at time t =30 s. Similar results are presented for sites B and C in Figs. 12 and 13, respectively. The residual values of $\Delta u / \sigma'_{m0}$ at point M for sites A, B, and C are 0.3, 0.4 and 1. At sites A and B, higher values of the ratio occur near the sides of the building, due to rocking. At site C, liquefaction occurs quickly (within 5 seconds from the start of the shaking) and expands across

the entire width and thickness of the soil layer. Fig. 14 plots the displacement time histories at all floors for the three buildings for the Kalamata excitation, and the IDI versus the building height for three different excitations. Note that although liquefaction occurs at site C, the damage at sites B and A appears to be higher. The softening of the soil layer very early during shaking at site C acts as a filtering mechanism leading to smaller horizontal displacements, but not necessarily smaller overall damage, as the increased differential movements among various columns cause again significant plastic deformation of beams. The deformed shapes of the building shown in Figs. 11, 12 and 13 (at time t = 30 s), do not represent the final stage, as additional deformation may occur during excess pore water pressure dissipation and consolidation of the soil layers.

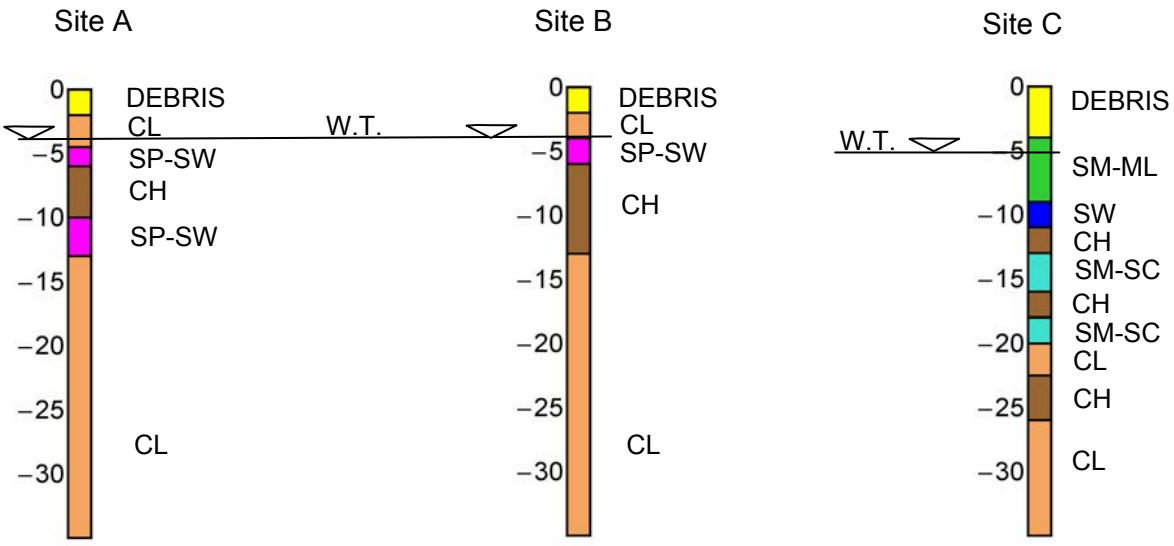

Figure 10: Soil profiles at sites A, B and C.

CONCLUSIONS

The effective stress method and an elasto-plastic constitutive soil model have been used to examine the effect of a liquefiable foundation soil layer on seismic damage of a typical building. The parameters of the constitutive model have been derived based on the relative density of the soil, estimated from corrected N-SPT values and the grain size distribution characteristics. The results of the seismic analysis of four different soil structure systems showed that the presence of a liquefiable layer may affect significantly the seismic behaviour and the damage of a structure. The typical, low-ductility 7-storey building investigated, experienced tolerable deformations at the typical soil profile, in which average soil properties are considered. In this case the Interstorey Drift Index (IDI) remained well below the critical values of 1%. At sites A, B and C, containing liquefiable soil layers with relative density 60%, 50% and 40%, respectively, the same 7-storey building developed significant damage and values of IDI well above 1%. Such deformations cannot be sustained by the low natural ductility of the older buildings designed by outdated older codes, such as the Greek Seismic Code of 1985. In addition to horizontal displacements, significant plastic deformation and bending was found in many beams located between the ground floor and the third floor. The conclusions regarding the behaviour of the superstructure are drawn from the analysis of the same building founded at four different sites. It is desirable to examine also the behaviour of other typical structures and the effect of the 3-D geometry of the structure on the seismic behaviour and damage. Finally, it is noted that the dynamic SSI interaction phenomena under the influence of excess pore water pressure and potential liquefaction are very complex and affected by several factors. The effective stress method can be a valuable tool in investigating the effect of such factors.

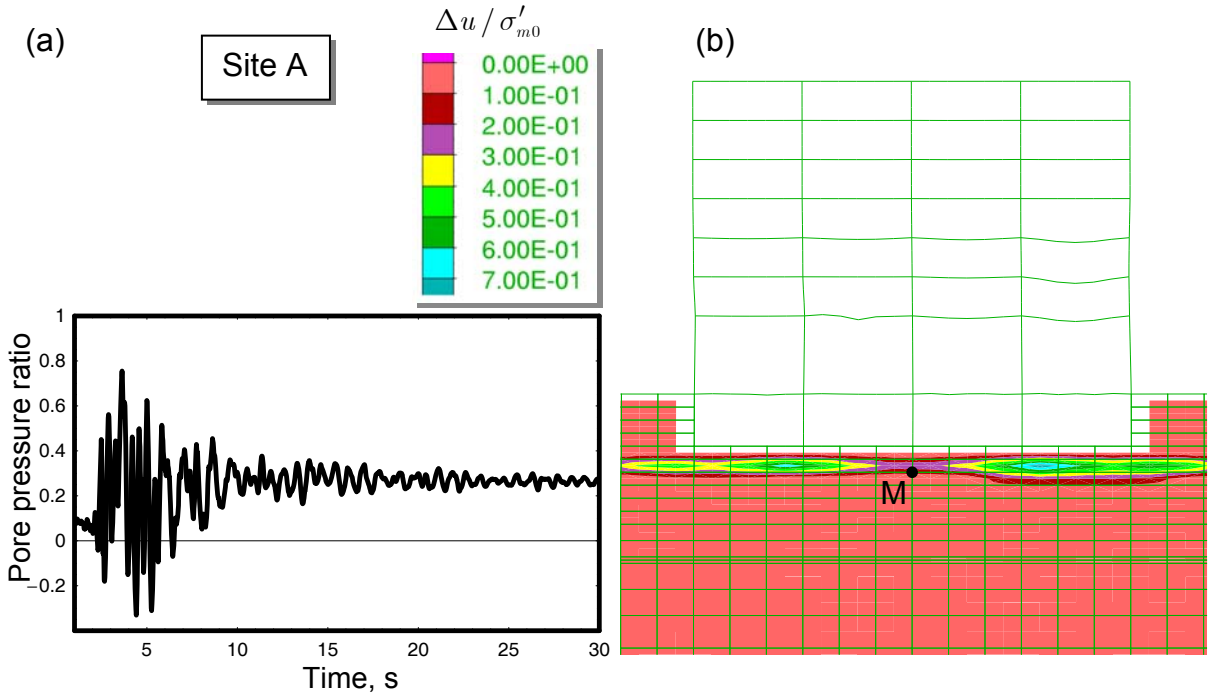

Figure 11. Site A: (a) Excess pore pressure ratio versus time at the middle of the liquefiable layer (Point M) and (b) Contours of excess pore pressure ratio within the liquefiable layer and deformed structure at time t = 30 s.

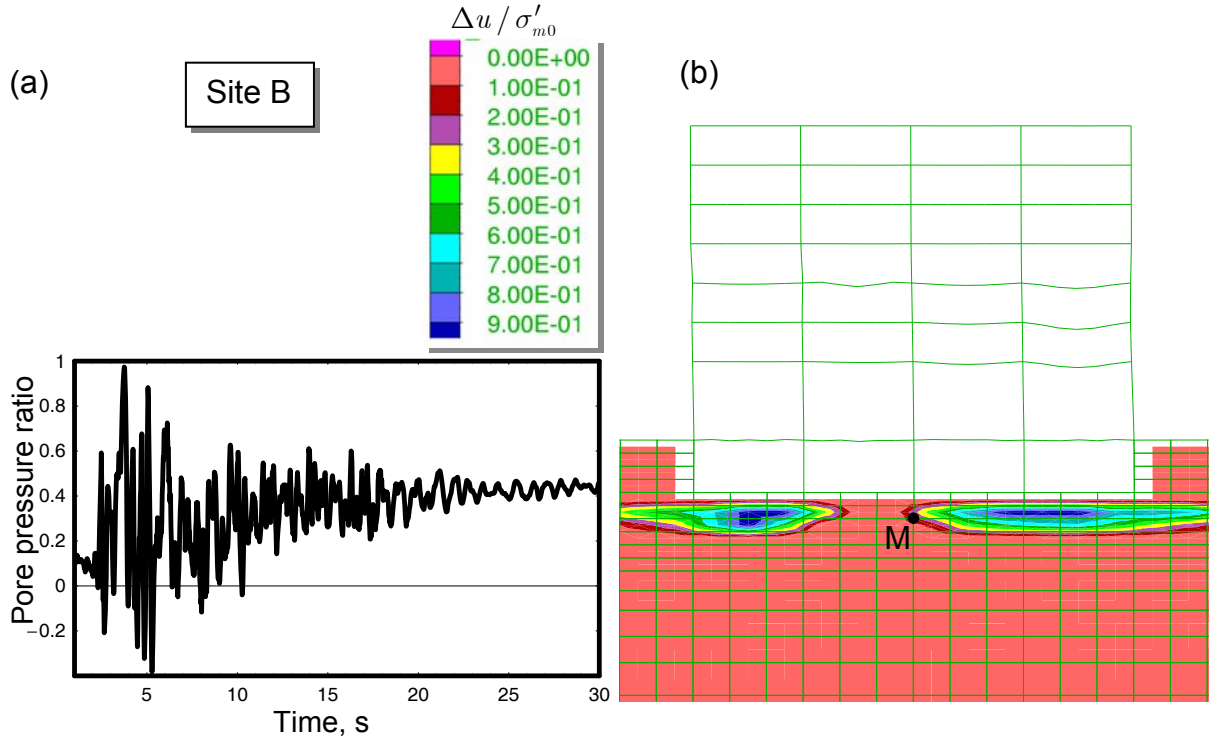

Figure 12. Site B: (a) Excess pore pressure ratio versus time at the middle of the liquefiable layer (Point M) and (b) Contours of excess pore pressure ratio within the liquefiable layer and deformed structure at time t = 30 s.

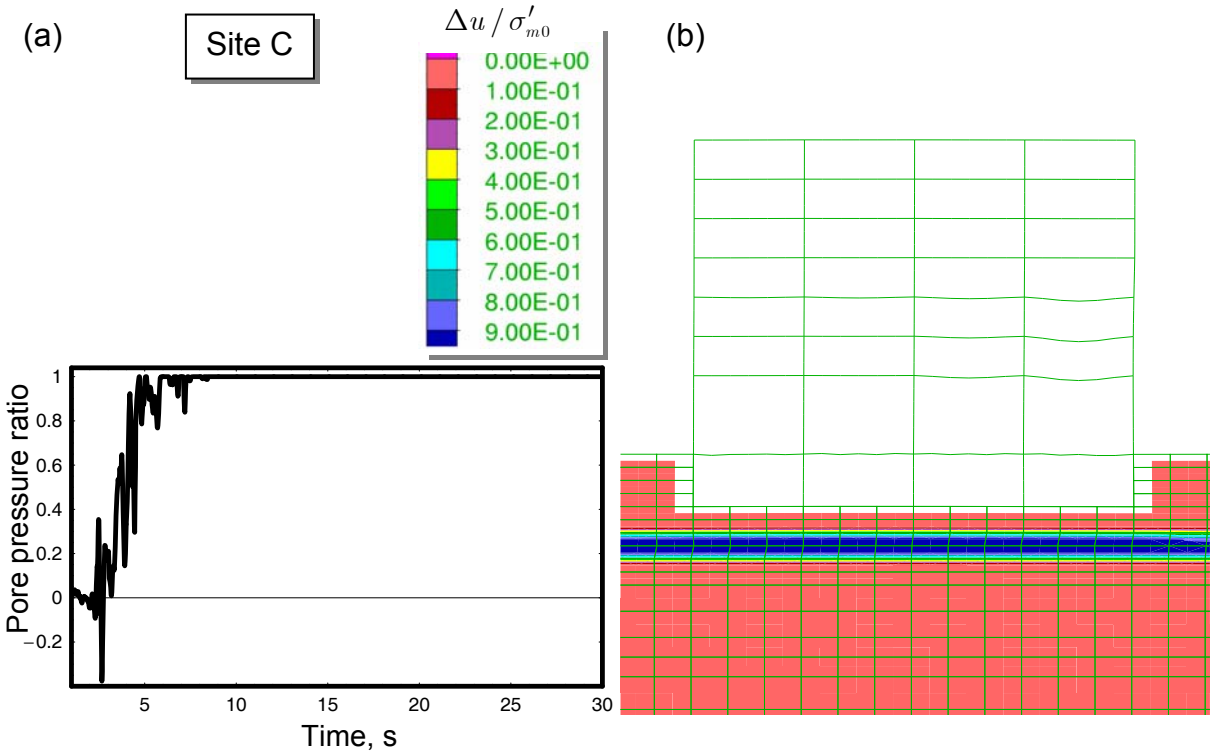

Figure 13. Site C: (a) Excess pore pressure ratio versus time at the middle of the liquefiable layer (Point M) and (b) Contours of excess pore pressure ratio within the liquefiable layer and deformed structure at time t = 30 s.

REFERENCES

Technical Chamber of Greece, "Utilization of the Microzonation Study of the City of Larissa", Larissa, 2000 (in Greek).

Arulmoli, K., Muraleetharan, M., Hossain, M and Fruth, L., "Verification of Liquefaction Analyses by Centrifuge Studies Laboratory Testing Program Soil Data Report", Report, The Earth Technology Corporation, Long Beach, California, 1992.

Bachmann, H., "Seismic Protection of Structures", Gourdas, Athens, 1998 (in Greek).

Castro, G., "Liquefaction of sands," Ph.D. Thesis, Harvard University, Harvard Soil Mechanics Series, No. 81, 1969.

Dakoulas, P. (2003), "Verification of a constitutive model for non-cohesive soils", Research Report, Univ. of Thessaly, Volos, Greece, 2003 (in Greek).

Dakoulas, P. and Gazetas, G., "Seismic Effective Stress Analysis of Caisson Quay Walls: Application to Kobe", Soils and Foundations, Vol. 45(4), 113-125, 2005.

DeAlba, P., Seed, H. B., & Chan, C. K., "Sand liquefaction in large scale simple shear tests", Journal of the Geotechnical Engineering Division, ASCE, Vol. 102, 9, pp 909-927, 1976.

EAK2000 (Greek Code for Seismic Design), O.A.S.P. & Society of Civil Engineers of Greece, Athens, 2000.

Pastor, M., O. Zienkiewicz, O., & Chan, C. H., "Generalized plasticity and the modeling of soil behavior", International J. of Numerical and Analytical Methods in Geomechanics, Vol. 14, pp. 151-190, 1990.

Pitilakis, K. and Tsotos, S., "Microzonation Study of the City of Larissa", Aristotle University of Thessaloniki, 1995 (in Greek).

Itasca, "FLAC", Computer Software, Manuals version 4, 2000.

Schnabel, P, Lysmer, J, and Seed, H.B., "SHAKE: Equiv. Linear Seismic Response Analysis of Horiz. Layered Soil Deposits", Computer Software Manual, 1972.

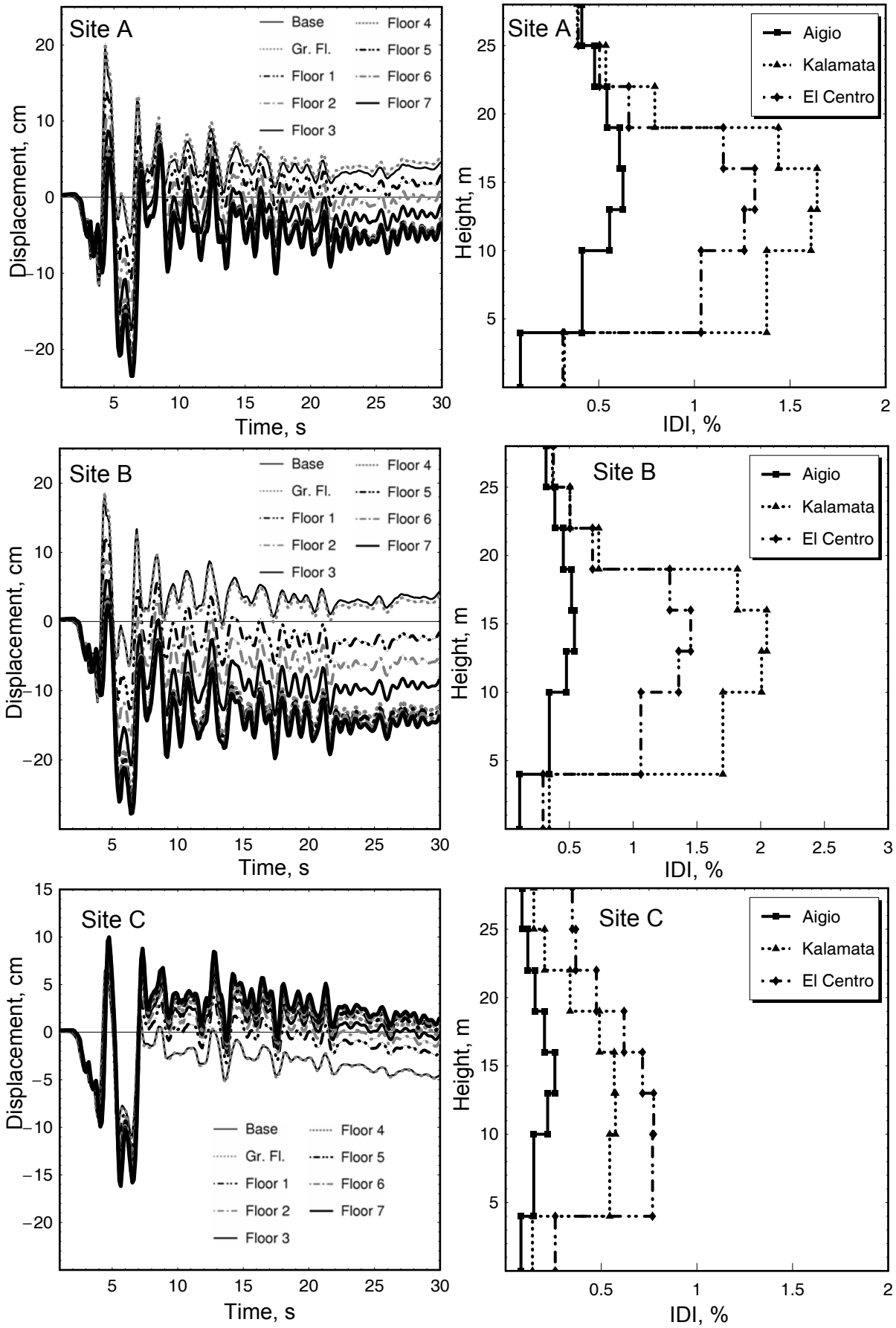

Figure 14. (a) Displacement time histories and (b) Interstory Drift Index along the building height for sites A, B and C.